The role of satellite observations in understanding the impact of El Niño on the carbon cycle: current capabilities and future opportunities

[Opinion piece]

The role of satellite observations in understanding the impact of El Niño on the carbon cycle: current capabilities and future opportunities

Paul I. Palmer

ORCID #: https://orcid.org/0000-0002-1487-0969

National Centre for Earth Observation, University of Edinburgh, UK

Keywords:

The 2015/2016 El Niño was the first major climate variation when there were a range of satellite observations that simultaneously observed land, ocean, and atmospheric properties associated with the carbon cycle. These data are beginning to provide new insights into the varied responses of land ecosystems to El Niño, but we are far from fully exploiting the information embodied by these data. Here, we briefly review the atmospheric and terrestrial satellite data that are available to study the carbon cycle. We also outline recommendations for future research, particularly the closer integration of satellite data with forest biometric datasets that provide detailed information about carbon dynamics on a range of timescales.

1 Introduction

Global mean atmospheric concentrations of carbon dioxide (CO_2) have increased by 40% from about 277 parts per million (ppm) in the late 19th century, prior to the advent of the industrial revolution, to present-day values of more than 400 ppm [Ciais et al, 2013]. Current atmospheric concentrations are now higher than any time at least in the past 800,000 years [Lüthi et al, 2008]. This unprecedented atmospheric rate of increase is primarily due to growing human activities: widespread combustion of fossil fuel, cement production to meet growing construction demands, and land use change to meet global demands for food and timber. These activities are embedded within a large and active natural biospheric cycle. Current estimates report that approximately 50% of CO_2 emissions are absorbed by the land biosphere and the oceans (e.g. Ballantyne et al, 2012, Barlow et al, 2015), but if this rate of absorption cannot be sustained we will be exposed to a larger atmosphere fraction of the additional CO_2 we emit.

Our current understanding of the land biosphere and how it responds to exogenous drivers is particularly uncertain, limited primarily by sparse ground-based measurements. Fig. 1 shows the distribution of continuous and flask samples of atmospheric CO_2 mole fraction collected by the US National Oceanic and Atmospheric Administration (NOAA, https://www.esrl.noaa.gov/gmd/ccgg/trends/global.html). Charles Keeling established a measurement site on Mauna Loa, Hawaii during the 1957 international geophysical year [Keeling, 1960], with the objective of understanding atmospheric variations of CO_2 on large spatial and temporal scales. Data collected at this site contributed to the scientific justification for the establishment of a global network. The NOAA network in its current form has large gaps in the tropics, reflecting the difficulty of maintaining a measurement programme over these regions. Nevertheless, the data from this network have since been a key source of information that underpin current understanding of the global carbon cycle

[Ciais et al, 2013]. Fig. 1 also shows latitude-time Hovmöller diagrams for the years surrounding the 1997/1988 and 2015/2016 El Niño events that illustrate a reduced form of the available information. By averaging over zonal bands we effectively discard longitudinal variations, allowing us to emphasize the latitude variations of CO_2 as a function of time. The atmospheric mole fraction data require the application of atmospheric transport models to infer the location and magnitude of the responsible net CO_2 fluxes (emissions minus uptake). The two Hovmöller diagrams shown by Fig. 1 illustrate the contrasting atmospheric CO_2 patterns associated with the different responses of the tropical carbon cycle to El Niño events (e.g. Page et al, 2002, Huijnen et al, 2016, Patra et al, 2017, Liu et al, 2017, Chylek et al, 2018).

Satellite observations of Earth's atmosphere and land surfaces have been available for decades, but we are now entering a new observational era for the carbon cycle in which we have (or soon will have) the capability to observe simultaneously many of its constituent components. What is particularly exciting is that these space-borne data are beginning to observe the atmosphere and land surface on spatial scales comparable with *in situ* ecological measurements.

Fig. 2 shows the Niño 3.4 sea surface temperature (SST) anomaly index, a common metric used to identify phases of the El Niño Southern Oscillation (ENSO). ENSO is a pan-tropical climate variation driven by gradients of equatorial SSTs over the Pacific. Under neutral conditions trade winds push warmer waters westward, piling it up in the western Pacific; during the La Niña phase of ENSO the neutral case is exaggerated resulting in a northward shift in the jet stream. During El Niño these trade winds weaken and the east-west SST gradient weakens with less upwelling of cooler, nutrient-rich water over the eastern Pacific that eventually impacts the local fishing industry. Changes in equatorial Pacific SSTs also result in a southward and intensified shift in the jet stream that effectively impacts weather patterns over the tropics. Fig. 2 shows the prominence of the 1982/83, 1997/1998, and 2015/2015 El Niño events [L'Heureux et al, 2017].

Fig. 2 also shows when different satellite data became available. The 2015/2016 El Niño was the first major climate variation that provided a natural showcase for these types of space-borne data. During this period we had access for the first time to simultaneous satellite-retrieved data to characterize photosynthesis (solar induced fluorescence, SIF), fire (active fire data, burned area, trace gases), leaf phenology (vegetation indices), hydrology (water storage inferred from gravitational anomalies), land surface temperature (respiration), and atmospheric CO_2 and other trace gases. The main purpose of this perspective is to highlight *some* of these data that can be and are being used to study the impacts of El Niño on the tropical carbon cycle. Section 2 describes individual types of relevant satellite data. We conclude in section 3 with a discussion about how to best use these large volumes of heterogeneous data to further basic knowledge about the tropical carbon cycle in the context of *in situ* measurements.

2 Satellite Observations Relevant to El Niño

Earth observing satellites are growing in number and variety, e.g. http://www.earthobservations.org. There is an ongoing challenge to exploit the vast amount of information satellite instruments produce every day in order to understand planet Earth.

Current satellite observations are beginning to challenge our fundamental knowledge of the carbon cycle, with the next generation of sensors being launched so they can play a role in determining global stock takes of carbon as part of the Paris Agreement. Analysis of these observations is an exemplar of the big data challenge that is now faced by many scientific disciplines.

Some satellite data have been available since the 1980s, e.g. thermal infrared (IR) anomalies to determine fires, land and sea surface temperature, and leaf phenology data such as leaf area index [National Academy of Sciences, 2008]. The start of the current century marked the advent of sensors that were sensitive to tropospheric chemistry, or more accurately our repurposing of instruments originally intended for monitoring ozone chemistry in the stratosphere. These have since been replaced by instruments dedicated to studying tropospheric chemistry, including gases and aerosols that are relevant to climate and air quality and by-products of combustion and biogenic emissions (e.g., Palmer, 2008, Surl et al, 2018). It is only in the last decade we have begun to see the launch of dedicated instruments that are focused on specific components of the land and ocean surfaces, e.g. soil moisture [Entekhabi et al, 2010, Kerr et al, 2010], ocean salinity [Kerr et al, 2010]. Table 1 shows an overview of satellite instruments relevant for understanding the response of tropical carbon cycle to El Niño.

Figs. 3 and 4 show the spatial and temporal distributions of a range of satellite observations relevant to studying the tropical carbon cycle. We show the August 2015 spatial distribution of atmospheric and land surface properties observed by satellite (Fig. 3) to illustrate some of the data available during the 15/16 El Niño.

Vegetation cover and phenology

Earth-observing satellites using optical and radar methods can detect land use and land use change. Optical remote sensing methods use the sun as its source, while radar and LiDAR sensors generate their own energy source and use backscatter as their signals. Optical data, with the latest Landsat-8 sensors using wavelengths spanning from the ultra-blue to the thermal, provide an assessment of forest canopy cover that can be used to derive estimates of the density and health of leaves [Roy et al, 2014]. Optical instruments cannot see through clouds, prevalent in the tropics, and cannot see below-canopy changes. Radar satellites use microwaves to penetrate through the canopy to determine forest structure. One application of these microwave data is to determine aboveground biomass using ground-based relationships between biomass from plot and LiDAR metrics. [Englhart et al, 2011]. However, the most sensitive L-band sensors saturate at values much less than the biomass densities commonly found over the tropics (~250 tonnes/ha) [Yu and Saatchi, 2016], although future missions will use the P-band that will increase the values at which the sensors saturate.

There are several remotely sensed vegetation indices of which the three most commonly used include the Normalized Difference Vegetation Index (NDVI), leaf area index (LAI), and enhanced vegetation index (EVI). These indices provide a crude estimate of canopy greenness that reflect changes in leaf area, chlorophyll content, and canopy structure (e.g., Huete et al, 2002). NDVI takes advantage that denser vegetation will reflect more at near-IR than visible wavelengths. It is mainly used as a quantitative metric of vegetation density, although recent studies have highlighted a possible role for forest stand age in NDVI

variations [Galvão et al, 2015]. LAI is the leaf area per unit ground area and is determined by the fraction of incoming photosynthetic active radiation between 0.4nm and 0.7nm absorbed by the plant canopy. EVI is defined similarly to NDVI but is more sensitive to higher biomass regions that are found in the tropics and the contributing wavelengths take into account atmospheric influences such as aerosol scattering. Fig. 3 shows the monthly mean distribution of EVI for August 2015 from the NASA Moderate Resolution Imaging Spectroradiometer (MODIS) aboard the NASA Aqua satellite. These data show the extent and density of vegetation across tropical ecosystems.

Hydrology

The ESA Soil Moisture Ocean Salinity (SMOS, Kerr et al, 2010) and JPL Soil Moisture Active Passive (SMAP, Entekhabi et al, 2010) both use L-band passive microwave remote sensing to estimate the amount of water in the top 5 cm of soil. Variations of soil moisture observed by SMOS or SMAP correspond closely to inputs from precipitation. Maximum rooting depths of vegetation are commonly used to characterize their susceptibility to drought (e.g. Fan et al, 2017). Tropical ecosystems, including grassland and savannah species, can develop rooting depths of 1-10s metres to reach the water table in response to the length of the dry season they experience. Consequently, changes in soil moisture in the top 5 cm rarely describe the limits of ecosystem access to groundwater. The Gravity Recovery and Climate Experiment (GRACE), launched in 2002, was originally intended to study variations in gravity [Tapley et al, 2004]. GRACE accurately measures the distance between its two satellites that are flown in tandem. A successful data product from GRACE has been the liquid water equivalent (LWE) thickness anomaly [Famiglietti and Rodell, 2013], which has been related to *changes* in the terrestrial water storage, an integrated measure of the water column, with an accuracy of 38 mm (15 mm) at a spatial scale of 500 km (1000 km) [Wahr et al, 2006]. Fig. 3 shows the monthly distribution of GRACE LWE for August 2015. The data show regions with positive water column anomalies over western Africa and negative water column anomalies over central Africa, over much of Brazil and over much of Southeast Asia and northern Australia. The negative water anomaly over Southeast Asia appears to have exacerbated the ongoing agricultural practices of draining peatlands over Indonesia by increasing the susceptibility of this fuel to combustion [Huijnen et al, 2016].

Fires

Landscape fire is an integral part of many tropical ecosystems. The most established satellite data product associated with fire is thermal IR anomalies. These data, measured since the 1980s, provide information on the location, extent, and to a lesser extent duration of actively burning landscape fires but nothing about the strength of a fire or about the fuel being burned. Newer products include fire radiative power [Wooster et al, 2005], which can be derived from more sophisticated sensors operating in the thermal IR, particularly those sensitive to the 3 to 5 micron spectral region. This product can be used to determine biomass combustion rates and totals, and to help determine pyroconvective injection heights that describe the maximum altitude reached by the emitted smoke due to intense surface heating (e.g., Gonzi et al, 2015, Paugam et al, 2016). Further developments include routine global burned area maps, which take advantage of the rapid changes in land surface reflectance (visible to shortwave IR) associated with the burning of vegetation and the surface deposition of charcoal and ash to identify daily updates to global burned area [Randerson et al, 2012].

The characteristics of the gases and aerosols emitted by fire depends on a number of factors [Akagi et al, 2011], e.g. fuel loading, fuel moisture and combustion phase (e.g. smouldering or flaming). Common trace gases that are used as markers for biomass burning include carbon monoxide (CO) and formaldehyde (HCHO). Measuring CO has the advantage that it has an atmospheric lifetime long enough that it is easily measured but short enough that surface emissions can be identified above a global background. The Measurement of Pollution In The Troposphere (MOPITT), launched in 1999, has since provided the science community with CO columns measured at thermal IR wavelengths that are most sensitive to the free troposphere (e.g., Edwards et al, 2004, Deeter et al, 2013). Past work has shown that biomass burning emissions rarely possess sufficient energy to be deposited directly into the free troposphere [Val Martin et al, 2010]. Consequently, CO ascends with larger-scale weather systems that result in a diluted signal away from the fire. Use of HCHO columns has the advantage that its short lifetime of a few hours means that it resides mostly in the lower troposphere close to the emission source [Gonzi et al, 2011]. HCHO has a primary emission source from combustion but also has a secondary source from the oxidation of a range of volatile organic compounds co-emitted by the fire, and by other processes – most notably from biogenic emissions of isoprene (e.g. Palmer et al, 2003, 2006). Separating the pyrogenic signal for HCHO requires additional data, e.g. thermal IR anomalies [Gonzi et al, 2011]. However, HCHO is only a weak absorber at UV wavelengths that are used to retrieve HCHO columns [Chance et al, 2000], and for less energetic fires HCHO will be chemically lost before it can be effectively observed. Fig. 3 shows monthly HCHO column distributions from the Dutch/Finnish Ozone Monitoring Instrument (OMI) [Levelt et al, 2017] aboard the NASA Aura for August 2015. As a (crude) effort to identify elevated HCHO columns from pyrogenic emissions we have retained columns that correspond to the location of active fires identified by thermal IR anomalies. The location of elevated columns indicates the location of fires, and the column values are a function of the characteristics of the fuel being burned. For instance, we expect HCHO columns to be lower over Central Africa where the main fuel is grassland savannas and savanna woodlands that generally have lower calorific content and are less densely packed than vegetation over tropical South America. There is also moderate burning over North Sumatra during August, but the spatial extent increases dramatically later in the El Niño event [Huijnen et al, 2016].

Solar-induced fluorescence

Absorption of incoming solar radiation by plant pigments drives photochemical reactions that eventually produce glucose as part of photosynthesis [Frankenberg and Berry, 2018]. Any excess energy is dissipated as heat or as fluorescence. Of the solar radiation absorbed, 20% is eventually dissipated as heat and 2% is emitted by SIF between 685-690 nm and 730-740 nm. The result is a small offset (typically <1%-2%) to the reflected sunlight that can be observed by satellite remote sensing in the 750 nm spectral range. Linking SIF with gross primary productivity is a key step that is being developed through biome-specific empirical relationships with data collected at flux tower sites (e.g. Frankenberg et al, 2016), building on mechanistic studies (see review by Frankenberg and Berry, 2018). SIF products are available from a range of imaging and spectroscopic instruments (e.g. GOME-2 [Joiner et al, 2013], GOSAT [Parazoo et al, 2013], OCO-2 [Sun et al, 2017]). Formal integration of these data with models is key to extracting the information, which is the subject of ongoing work (e.g. Norton et al, 2018). Fig. 3 shows the monthly distribution of SIF for August 2015 from

the GOME-2B satellite aboard the ESA/EUMETSAT MetOp satellite. It has an equatorial overpass time of 0930 local time by which time vegetation will have received approximately three hours of sunlight. Values will change with, for example, vegetation type, density, and health. They could also be affected by residual cloud contamination by virtue of their pixel size (40km x 80km), an effect that is less prominent with instruments with finer spatial resolution, e.g. GOSAT and OCO-2 (Table 1).

Atmospheric observations

The global atmosphere is a nearly passive component of the carbon cycle, with global atmospheric CO_2 mass mainly responding to changes in land and ocean surface fluxes; in practice, there is also a small, diffuse CO_2 source from the oxidation of reduced carbon [Suntharalingam et al, 2005]. Atmospheric mixing results in information, associated with these atmospheric signals, being irreversibly lost so that atmospheric transport cannot be inverted deterministically. This places limits on our ability to estimate geographical distributions of CO_2 fluxes from observed atmospheric variations of CO_2. With such imperfect knowledge of the atmosphere, Bayesian inference methods are typically used that take advantage of *a priori* information from flux models (describing static inventories and dynamical land surface models) that are informed by, for example, by field campaigns.

It is because of its mixing properties that the atmosphere is an effective integrator. The original placement of ground-based instruments to measure atmospheric CO_2, indeed, relied on those atmospheric properties. But even these properties cannot overcome the measurement gaps over the tropics (Fig. 1). Satellite observations are ideal to fill in those gaps but substantive progress has only been made in the last decade with the launch of the Japanese Greenhouse gases Observing SATellite (GOSAT) in 2009 [Kuze et al, 2009] and the NASA Orbiting Carbon Observatory (OCO-2) in 2014 [Eldering et al, 2017]. Both instruments reside in a sun-synchronous orbit with an early afternoon equatorial overpass time of 13:30. They observe atmospheric CO_2 using three modes: nadir mode that measures the column in the local nadir; sunglint mode that takes advantage of the high signal-to-noise from specular reflection off ocean and (to a lesser extent) land surfaces; and target mode that locks onto a point on the surface and tracks it while flying overhead. The challenge has been to develop the short-wave IR sensor technology that is sufficiently precise to observe the small (typically < a percent) changes in the CO_2 column from surface fluxes. Thermal IR retrieval of atmospheric CO_2 have been available for a lot longer, but they are most sensitive to change in CO_2 above the free troposphere. Relating these thermal IR data to surface fluxes relies more on atmospheric transport models (particularly vertical motion) than observations at short-wave IR wavelengths that are more sensitive to changes in CO_2 in the lower troposphere. Fig. 3 shows the monthly distribution of CO_2 dry-air mole fraction observations (X_{CO2}) from GOSAT for August 2015. X_{CO2} values over the tropics for this month range by 6 ppm (1.5% of the 400 ppm background) illustrating the demanding precision requirement of this measurement. Fig. 3 also shows the *a posteriori* fluxes that have been inferred for August 2015 using observations from that month and later months, which clearly show large coherent regions of CO_2 emissions and uptake. These fluxes appear smoothed because the data density supports independent flux estimates on spatial scales of O(500-1000 km).

These data are not a panacea for carbon cycle science. The main advantage of satellite data over the ground-based data is that they have global coverage, including coverage over

tropical ecosystems that have largely been unobserved. A disadvantage is that individual data retrievals are relatively noisy compared to the ground-based measurements. This is because our signal, i.e. fresh surface fluxes, represent (at most) a variation of a few percent atop a large column abundance that places demanding requirements on the measurement precision. One advantage of the column nature of these satellite data is that they are less sensitive than vertically resolved measurements to model errors associated with vertical mixing [Olsen and Randerson, 2004]. The disadvantage is that a column is generally a superposition of different geographical CO_2 fluxes atop of background that has slow and fast modes of variability to due to atmospheric growth and weather [Palmer et al, 2008].

Substantial efforts have been made to minimize X_{CO2} systematic errors, particularly on spatial scales between 100-1000 km, which will alias themselves as erroneous CO_2 fluxes. For example, the Total Carbon Column Observing Network (TCCON, Wunch et al, 2011), comprising upward-viewing FTIR instruments that are calibrated to a common standard (Fig. 1), was established to help provide anchor points for satellite data. Satellite column retrievals of CO_2 are now moving to the scientific forefront (e.g., Liu et al, 2017) as challenges associated with measurement uncertainties and regional biases are beginning to be addressed.

Understanding the contribution of land biosphere emissions to observed variations in atmospheric CO_2 remains a key science challenge (see Pinty et al, 2017 for a discussion of the counter focus of isolating anthropogenic CO_2 contributions). There is no single effective approach to link these variations to individual biophysical processes. From an atmospheric perspective, there are several potential reactive trace gases (atmospheric lifetimes << a few months) that could be used to help separate or at least help improve understanding of the relative importance of biomass burning, anthropogenic activities, and land biosphere fluxes. Observed atmospheric variations of these reactive gases over the tropics are interesting in their own right, but together can help identify combustion sources from biomass burning (e.g. CO, HCHO), and anthropogenic activity (nitrogen dioxide, ethane). By virtue of their absence, these gases can help isolate land biosphere fluxes. Observed variations of other gases such as carbonyl sulphide could also point to photosynthesis [Berry et al, 2013]. Clearly, a multi-species analysis is needed to disentangle anthropogenic, pyrogenic, and biospheric contributions to atmospheric CO_2. This is an area that has not yet been seriously attempted because of a lack of available data and expertise, but this situation is beginning to change (e.g. Fortems-Cheiney, 2012).

3 Future opportunities

We live in an era in which many environmental variables are now observed by satellite sensors. These data include a wide range of atmospheric trace gases and land-surface properties relevant to the carbon cycle. However, interpretation of these data is arguably still in its infancy, and, with a few notable exceptions, we have only achieved piecemeal analysis of individual data sets. Considerable information resides in the integration of different data, allowing us to make further inroads into answering the biggest scientific questions associated with the tropical carbon cycle.

In the previous section, we showed examples of individual satellite datasets for August 2015 (Fig. 3) as they were introduced. As discussed above, inferring CO_2 fluxes from satellite data

over the tropics is an important first step towards understanding the impact of climate variation on tropical ecosystems and how they can feedback to climate. Although the datasets shown in Fig. 3 are only a subset of the available information (consider additional variables and the time dimension of these data), we find many similarities in the spatial distributions of these variables, as expected. Fig. 4 shows an example of temporal variations of land surface properties and *a posteriori* CO_2 fluxes over northern tropical Asia. These variations illustrate how different factors that influence the tropical terrestrial carbon cycle (e.g. leaf phenology, photosynthesis, fire, drought) covary. Collectively, these data have the potential to answer fundamental questions about the tropical carbon cycle. What is the impact of drought on photosynthesis? Can we distinguish between the role of fire and drought ecosystem level CO_2 fluxes? Can we distinguish between carbon emissions from vegetation and soil in anomalously dry and hot environments?

To reach beyond the simple comparisons shown in Fig. 3 and Fig. 4 we have to formally integrate different data using computational models. Models can range from simple falsifiable hypotheses to link a few model components to more comprehensive large-scale atmosphere-bio-physical models. Scientific insights have been gained already from both approaches. Linking models to the data is a key step. Not all land biosphere models are sufficiently developed to take full advantage of available satellite data, but rapid progress is being made (e.g. Norton et al, 2018). Similarly, atmospheric transport models have in the past used simplified flux inventories or simply using output from land biosphere models, but this is also changing. Once atmosphere-biosphere models have been developed so they can be confronted by land surface and atmospheric satellite remote sensing data the next step is to statistically fit the model to the data, taking into account model and measurement uncertainties. This statistical approach essentially describes a weighted least-squares fit of the model to the data.

For the purpose of readability of this perspective we will ignore the details of the various fitting approaches but suffice to say techniques exist and are well established. Previous studies have mostly inferred time-dependent surface fluxes of CO_2 (e.g. Fig. 3) but this place limits on our furthering knowledge of the land biosphere, i.e. it certainly does not improve our predictive capability. However, this approach serves as an intermediary objective. The ultimate objective must be to estimate model parameters (e.g. light sensitivity) that describe flux variations that subsequently drive atmospheric CO_2 variations. Model parameter estimation has been attempted by various studies but mostly with ground-based flux tower data (e.g. Wang et al, 2007). Reducing the large and heterogeneous data volumes available to us from satellite introduces its own challenges, but we anticipate that the richness of these data will support a larger number of estimated model parameters than from using only ground-based data. Nevertheless, we argue that model development should include the maximum (minimum) number of (un)falsifiable parameters, determined by the quality and volume of data, necessary to describe the key variations of a system [Smith et al, 2014], an approach which readily allows identification of model error.

Satellite data alone will not address the major uncertainties associated with the tropical carbon cycle and how it responds to climate variations. For decades, terrestrial ecologists have painstakingly collected a range of pan-tropical forest biometric data (e.g. mortality, respiration, soil carbon, leaf litter) from sample plots across the major continents (e.g., Mahli et al, 2015, Feldpausch et al, 2016). These data are sparse but accurate and provide

insights into biomass dynamics on relatively small spatial and long temporal scales. The impact of the 2015/2016 El Niño will likely result in mortality rates and reduced ecosystem functioning that will not be fully realized for many years to come. It will be difficult to assess these impacts using current satellite data. Consequently, to develop a more comprehensive understanding of the tropical carbon cycle it is critical all available data be used. Harmonizing these biometric data, some of which describe changes on decadal timescales, with the satellite data represents a scientific challenge but also an opportunity to build collaborations between terrestrial ecologists, satellite remote sensing scientists, and atmospheric scientists.

Looking to the future, there are a number of satellite instruments that will eventually replace GOSAT and OCO-2 using similar orbits (Table 1). GOSAT-2 is due for launch in ~2018 the French-UK bilateral MicroCarb is due to be launched in ~2021, and the CO_2 component to the Copernicus service (currently being defined) will likely include multiple satellites and be launched after 2025. Major innovations will come from the adopted orbit and technologies. OCO-3 is due to become an instrument aboard the International Space Station (ISS) sometime in 2019. The ISS is in an inclined orbit so it precesses between ±51.6 degrees latitude, which could lead to more clear-sky scenes over the tropics (Palmer et al, 2011). The NASA GeoCarb, scheduled for launch in 2022, will be launched in a geostationary orbit above the Americas with a vantage point that covers ±50 degrees latitude that covers much of North and South America; similar complementary concepts have been proposed for Asia and Africa. Concepts that use active remote sensing to measure atmosphere CO_2 (e.g. NASA ASCENDS) are not subject to the limits of available reflected sunlight and will provide data during day and night. Active remote sensing concepts will at least double the volume of atmospheric CO_2 data over the tropics. These data will have a spatial resolution much smaller than current atmospheric transport models, so they will likely need to averaged to model grid scales to ensure a meaningful comparison. Recall that columns are a superposition of geographical fluxes from various times, so that measuring CO_2 columns over the Amazon basin during night, for example, will reflect values from earlier times of the day and from far upwind. BIOMASS and FLEX are two ESA flagship Earth Explorer missions. Both build on our observing capabilities with current satellites. BIOMASS will employ the P-band to determine the amount of biomass and carbon stored in forests. As discussed earlier, using the P-band avoids the signal saturating at biomass values that are much lower than found over tropical ecosystems. BIOMASS is due for launch in 2020. Fluorescence Explorer (FLEX) mission, due for launch in 2022, includes sensors to measure fluorescence, hyperspectral reflectance, and canopy temperature with a focus on addressing spatial and temporal scaling issues associated with comparing measurements collected at towers and by satellites. FLEX will fly in tandem with the Sentinel 3 satellite that also has complementary optical and thermal sensors, allowing a more integrated assessment of plant functioning.

We may very well be at the start of a golden age of observing the tropical carbon cycle using satellite instruments. Major advances in scientific understanding will come from integrating interrelated information collected from different satellite instruments, and more broadly from strengthening links between terrestrial ecologists, satellite remote sensing experts, and atmospheric scientists.

Competing interest: None.

Acknowledgements:
Thanks to Liang Feng for providing the *a posteriori* CO_2 flux estimates corresponding to the GOSAT data, and to Martin Wooster, Hartmut Bösch, and Sassan Saatchi for providing comments on an early version of this draft and input to Table 1. We gratefully acknowledge Gonzalo González Abad (Harvard-Smithsonian Center for Astrophysics), Joanna Joiner (NASA GSFC), and the science teams of MODIS, GRACE, GOME-2, and GOSAT to providing their data. We also acknowledge NOAA ESRL/GMD and all the contributing measurement teams for the CO_2 mole fraction data plotted in Fig. 1 (https://www.esrl.noaa.gov/gmd/dv/data/). The NASA OMI HCHO data (OMHCHOv003) are available from the NASA Data and Information Services Center; the GOME-2 SIF data are available NASA Aura Validation Data Center; the GRACE data are available from JPL Physical Oceanography Distributed Active Archive Data Center; MODIS EVI data are available from the Land Processes Distributed Active Archive Center; and the GOSAT v7.1 XCO2 full-physics retrievals are from the University of Leicester.

Funding: PIP is funded by the NERC National Centre for Earth Observation (grant # PR140015).

References

Akagi, S. K., Yokelson, R. J., Wiedinmyer, C., Alvarado, M. J., Reid, J. S., Karl, T., Crounse, J. D., and Wennberg, P. O., Emission factors for open and domestic biomass burning for use in atmospheric models, Atmos. Chem. Phys., doi:10.5194/acp-11-4039-2011, 2011.

Ballantyne, A. P., Alden, C. B., Miller, J. B., Tans, P. P., and White, J. W. C.: Increase in observed net carbon dioxide uptake by land and oceans during the past 50 years, Nature, doi:10.1038/nature11299, 2012.

Barlow, J. M., Palmer, P. I., Bruhwiler, L. M., and Tans, P., Analysis of CO_2 mole fraction data: first evidence of large-scale changes in CO_2 uptake at high northern latitudes, Atmos. Chem. Phys., 15, doi:10.5194/acp-15-13739-2015, 2015.

Berry, J., et al, A coupled model of the global cycles of carbonyl sulfide and CO_2: A possible new window on the carbon cycle, Journal of Geophysical Research: Biogeosciences, doi: 10.1002/jgrg.20068, 2013.

Chance, K., P. I. Palmer, R. V. Martin, R. J. D. Spurr, T. P. Kurosu, and D. J. Jacob, Satellite observations of formaldehyde over North America from GOME, Geophys. Res. Lett, doi:10.1029/2000GL011857, 2000.

Chylek, P., P. Tans, J. Christy, and M. K. Dubey, The carbon cycle response to two El Nino types: an observational study, *Env. Res. Lett*., doi: 10.1088/1748-9326/aa9c5b, 2018.

Ciais, P., C. Sabine, G. Bala, L. Bopp, V. Brovkin, J. Canadell, A. Chhabra, R. DeFries, J. Galloway, M. Heimann, C. Jones, C. Le Quéré, R.B. Myneni, S. Piao and P. Thornton, 2013: Carbon and Other Biogeochemical Cycles. In: Climate Change 2013: The Physical Science

Basis. Contribution of Working Group I to the Fifth Assessment Report of the Intergovernmental Panel on Climate Change [Stocker, T.F., D. Qin, G.-K. Plattner, M. Tignor, S.K. Allen, J. Boschung, A. Nauels, Y. Xia, V. Bex and P.M. Midgley (eds.)]. Cambridge University Press, Cambridge, United Kingdom and New York, NY, USA.

Deeter, M. N., S. Martínez-Alonso, D. P. Edwards, L. K. Emmons, J. C. Gille, H. M. Worden, J. V. Pittman, B. C. Daube, and S. C. Wofsy, Validation of MOPITT Version 5 thermal-infrared, near-infrared, and multispectral carbon monoxide profile retrievals for 2000–2011, J. Geophys. Res. Atmos., doi:10.1002/jgrd.50272, 2013.

Edwards, D. P., et al. Observations of carbon monoxide and aerosols from the Terra satellite: Northern Hemisphere variability, J. Geophys. Res., doi:10.1029/2004JD00472, 2004.

Eldering, A., et al, The Orbiting Carbon Observatory-2: first 18 months of science data products, Atmos. Meas. Tech., doi:10.5194/amt-10-549-2017, 2017.

Englhart, S. and Keuck, V. and Siegert, F., Aboveground biomass retrieval in tropical forests —The potential of combined X- and L-band SAR data use, Remote Sensing of Environment, doi:10.1016/j.rse.2011.01.008, 2011.

Entekhab, D. et al, The Soil Moisture Active Passive (SMAP) Mission, Proceedings of the IEEE, doi:10.1109/JPROC.2010.2043918, 2010.

Famiglietti, James S. and Rodell, Matthew, Water in the balance, Science, doi:10.1126/science.1236460, 2013.

Fan, Ying and Miguez-Macho, Gonzalo and Jobbágy, Esteban G. and Jackson, Robert B. and Otero-Casal, Carlos, Hydrologic regulation of plant rooting depth, Proc Natl Acad Sci USA, doi:10.1073/pnas.1712381114, 2017.

Feldpausch TR, et al, Amazon forest response to repeated droughts. Global Biogeochemical Cycles. doi:10.1002/2015gb005133, 2016.

Feng, L., et al, Consistent regional fluxes of CH_4 and CO_2 inferred from GOSAT proxy XCH4 : XCO2 retrievals, 2010–2014, Atmos. Chem. Phys., doi:10.5194/acp-17-4781-2017, 2017.

Fortems-Cheiney, A., Chevallier, F., Pison, I., Bousquet, P., Saunois, M., Szopa, S., Cressot, C., Kurosu, T. P., Chance, K., and Fried, A.: The formaldehyde budget as seen by a global-scale multi-constraint and multi-species inversion system, *Atmos. Chem. Phys*., doi:10.5194/acp-12-6699-2012, 2012.

Frankenberg, C. and D. Drewry and S. Geier and M. Verma and P. Lawson and J. Stutz and K. Grossmann, Remote sensing of solar induced Chlorophyll Fluorescence from satellites, airplanes and ground-based stations, 2016 IEEE International Geoscience and Remote Sensing Symposium (IGARSS), doi:10.1109/IGARSS.2016.7729436, 2016.

Frankenberg, Christian and Berry, J, Solar Induced Chlorophyll Fluorescence: Origins, Relation to Photosynthesis and Retrieval, Reference Module in Earth Systems and Environmental Sciences, ISBN 9780124095489, doi: 10.1016/B978-0-12-409548-9.10632-3, 2018.

Galvão L. S., J. R. dos Santos, R. Dal'Agnol da Silva, C. V. da Silva, Y. M. Moura, and F. M. Breunig, Following a site-specific secondary succession in the Amazon using Landsat CDR product and field inventory data, *Int. J. Remote. Sens*., doi:10.1080/01431161.2014.999879, 2015.

Gonzi, S., P. I. Palmer, M. P. Barkley, I. De Smedt, and M. Van Roosendael, Biomass burning emission estimates inferred from satellite column measurements of HCHO: sensitivity to co-emitted aerosol and injection height, Geophys. Res. Lett., doi:10.1029/2011GL047890, 2011.

Gonzi, S., Palmer, P. I., Paugam, R., Wooster, M., and Deeter, M. N., Quantifying pyroconvective injection heights using observations of fire energy: sensitivity of spaceborne observations of carbon monoxide, Atmos. Chem. Phys., doi:10.5194/acp-15-4339-2015, 2015.

Huete, A and Didan, K and Miura, T and Rodriguez, E. P and Gao, X and Ferreira, L. G, Overview of the radiometric and biophysical performance of the MODIS vegetation indices, Remote Sensing of Environment, doi:10.1016/S0034-4257(02)00096-2, 2002.

Huijnen, V. and Wooster, M. J. and Kaiser, J. W. and Gaveau, D. L. A. and Flemming, J. and Parrington, M. and Inness, A. and Murdiyarso, D. and Main, B. and van Weele, M., Fire carbon emissions over maritime southeast Asia in 2015 largest since 1997, doi:10.1038/srep26886, 2016.

Joiner, J., Guanter, L., Lindstrot, R., Voigt, M., Vasilkov, A. P., Middleton, E. M., Huemmrich, K. F., Yoshida, Y., and Frankenberg, C.: Global monitoring of terrestrial chlorophyll fluorescence from moderate-spectral-resolution near-infrared satellite measurements: methodology, simulations, and application to GOME-2, Atmos. Meas. Tech., doi:10.5194/amt-6-2803-2013, 2013.

Keeling, C. D. The concentration and isotopic abundances of carbon dioxide in the atmosphere, Tellus, 12 (2), 1960.

Kerr, Y. H., Waldteufel, P., Wigneron, J.-P., Delwart, S., Cabot, F., Boutin, J., Escorihuela, M. J., Font, J., Reul, N., Gruhier, C., Juglea, S. E., Drinkwater, M. R., Hahne, A., Martin-Neira, M., and Mecklenburg, S.: The SMOS Mission: New Tool for Monitoring Key Elements of the Global Water Cycle, Proceedings of the IEEE, doi:10.1109/JPROC.2010.2043032, 2010.

Kuze, Akihiko and Suto, Hiroshi and Nakajima, Masakatsu and Hamazaki, Takashi, Thermal and near infrared sensor for carbon observation Fourier-transform spectrometer on the Greenhouse Gases Observing Satellite for greenhouse gases monitoring, Applied Optics, doi:10.1364/AO.48.006716, 2009.

Levelt, P., et al, The Ozone Monitoring Instrument: Overview of twelve years in space, Atmos. Chem. Phys. Discuss., doi:10.5194/acp-2017-487, in review, 2017.

L'Heureux, M.L., et al, Observing and Predicting the 2015/16 El Niño. Bull. Amer. Meteor. Soc., 98, 1363–1382, doi:10.1175/BAMS-D-16-0009.1, 2017

Liu, J. et al, Contrasting carbon cycle responses of the tropical continents to the 2015–2016 El Niño, Science, doi:10.1126/science.aam5690, 2017.

Lüthi, D. et al, High-resolution carbon dioxide concentration record 650,000–800,000 years before present, Nature, doi:10.1038/nature06949, 2008.

Malhi, Y. et al, The linkages between photosynthesis, productivity, growth and biomass in lowland Amazonian forests. Glob Change Biol, doi:10.1111/gcb.12859, 2015.

National Academy of Sciences, Earth observations from space: the first 50 years of scientific achievements, The National Academies Press, ISBN 978-0-309-11095-, doi:10.17226/11991, 2008.

Norton, A. J., Rayner, P. J., Koffi, E. N., and Scholze, M.: Assimilating solar-induced chlorophyll fluorescence into the terrestrial biosphere model BETHY-SCOPE v1.0: model description and information content, *Geosci. Model Dev.*, https://doi.org/10.5194/gmd-11-1517-2018, 2018.

Olsen, S. C., and J. T. Randerson, Differences between surface and column atmospheric CO2 and implications for carbon cycle research, J. Geophys. Res., doi:10.1029/2003JD003968, 2004.

Page, Susan E. and Siegert, Florian and Rieley, John O. and Boehm, Hans-Dieter V. and Jaya, Adi and Limin, Suwido, The amount of carbon released from peat and forest fires in Indonesia during 1997, Nature, doi:10.1038/nature01131, 2002.

Palmer, P. I., D. J. Jacob, A. M. Fiore, R. V. Martin, K. Chance, and T. P. Kurosu, Mapping isoprene emissions over North America using formaldehyde column observations from space, J. Geophys. Res., doi: 10.1029/2002JD002153, 2003.

Palmer, P. I., D. S. Abbot, T-M. Fu, D. J. Jacob, K. Chance, T. Kurosu, A. Guenther, C. Wiedinmyer, J. Stanton, M. Pilling, S. Pressley, B. Lamb, and A. L. Sumner, Quantifying the seasonal and interannual variability of North American isoprene emissions using satellite observations of formaldehyde column, *J. Geophys. Res.*, doi:10.1029/2005JD006689, 2006.

Palmer, P. I., Quantifying sources and sinks of trace gases using space-borne measurements: current and future science, Phil. Trans. R. Soc. A. doi:10.1098/rsta.2008.0176, 2008.

Palmer, P. I., Barkley, M. P., and Monks, P. S.: Interpreting the variability of space-borne CO_2 column-averaged volume mixing ratios over North America using a chemistry transport model, Atmos. Chem. Phys., doi:10.5194/acp-8-5855-2008, 2008.
Palmer, P. I., Feng, L., and Bösch, H., Spatial resolution of tropical terrestrial CO_2 fluxes inferred using space-borne column CO_2 sampled in different earth orbits: the role of spatial error correlations, *Atmos. Meas. Tech.*, doi:10.5194/amt-4-1995-2011, 2011.

Parazoo, N. C., Bowman, K., Frankenberg, C., Lee, J. E., Fisher, J. B., Worden, J., et al. Interpreting seasonal changes in the carbon balance of southern Amazonia using measurements of X_{CO2} and chlorophyll fluorescence from GOSAT. Geophysical Research Letters, doi:10.1002/grl.50452, 2013.

Patra, P. K. et al, The Orbiting Carbon Observatory (OCO-2) tracks 2–3 peta-gram increase in carbon release to the atmosphere during the 2014–2016 El Niño, doi:10.1038/s41598-017-13459-0, 2017.

Paugam, R., Wooster, M., Freitas, S., and Val Martin, M.: A review of approaches to estimate wildfire plume injection height within large-scale atmospheric chemical transport models, Atmos. Chem. Phys., doi:10.5194/acp-16-907-2016, 2016.

Pinty B., et al, An Operational Anthropogenic CO_2 Emissions Monitoring & Verification Support capacity - Baseline Requirements, Model Components and Functional Architecture, doi: 10.2760/08644, European Commission Joint Research Centre, EUR 28736 EN, 2017.

Randerson, J. T., Y. Chen, G. R. van derWerf, B. M. Rogers, and D. C. Morton, Global burned area and biomass burning emissions from small fires, J. Geophys. Res., doi:10.1029/2012JG002128, 2012.

Rayner, N. A., D. E. Parker, E. B. Horton, C. K. Folland, L. V. Alexander, D. P. Rowell, E. C. Kent, and A. Kaplan, Global analyses of sea surface temperature, sea ice, and night marine air temperature since the late nineteenth century, J. Geophys. Res., doi:10.1029/2002JD002670, 2003.

Roy, D. P. et al, Landsat-8: Science and product vision for terrestrial global change research, Remote Sensing of Environment, doi:10.1016/j.rse.2014.02.001, 2014.

Smith, M. J., et al, Changing how Earth System Modelling is done to provide more useful information for decision making, science and society, Bulletin of the American Meteorological Society, doi:10.1175/BAMS-D-13-00080.1, 2014

Sun, Y. et al, OCO-2 advances photosynthesis observation from space via solar-induced chlorophyll fluorescence, Science, doi:10.1126/science.aam5747, 2017.

Suntharalingam, P., J. T. Randerson, N. Krakauer, J. A. Logan, and D. J. Jacob, Influence of reduced carbon emissions and oxidation on the distribution of atmospheric CO_2: Implications for inversion analyses, *Global Biogeochem. Cycles*, doi: 10.1029/2005GB002466, 2005.

Surl, L., Palmer, P. I., and González Abad, G.: Which processes drive observed variations of HCHO columns over India?, *Atmos. Chem. Phys.*, doi:10.5194/acp-18-4549-2018, 2018.

Tapley, B. D., S. Bettadpur, M. Watkins, and C. Reigber, The gravity recovery and climate experiment: mission overview and early results, Geophy. Res. Lett, doi: 10.1029/2004GL019920, 2004.

Val Martin, M., Logan, J. A., Kahn, R. A., Leung, F.-Y., Nelson, D. L., and Diner, D. J.: Smoke injection heights from fires in North America: analysis of 5 years of satellite observations, Atmos. Chem. Phys., doi:10.5194/acp-10-1491-2010, 2010.

Wahr, J., S. Swenson, and I. Velicogna, Accuracy of GRACE mass estimates, Geophys. Res. Lett., doi:10.1029/2005GL025305, 2006.

Wang, Y, P., Baldocchi, D., Leuning, R., Falge, E., and Vesala, T., Estimating parameters in a land-surface model by applying nonlinear inversion to eddy covariance flux measurements from eight FLUXNET sites. Global Change Biology, doi:10.1111/j.1365-2486.2006.01225.x, 2007.

Wooster, M. J., G. Roberts, G. L. W. Perry, and Y. J. Kaufman, Retrieval of biomass combustion rates and totals from fire radiative power observations: FRP derivation and calibration relationships between biomass consumption and fire radiative energy release, J. Geophys. Res., doi:10.1029/2005JD006318, 2005.

Wunch, D. et al, The Total Carbon Column Observing Network, Philosophical Transactions of the Royal Society A: Mathematical, Physical and Engineering Sciences, doi:10.1098/rsta.2010.0240, 2010.

Yu, Y, and S. Saatchi, Sensitivity of L-band SAR backscatter to aboveground biomass of global forests, Remote Sens., doi:10.3390/rs8060522, 2016.

Figures

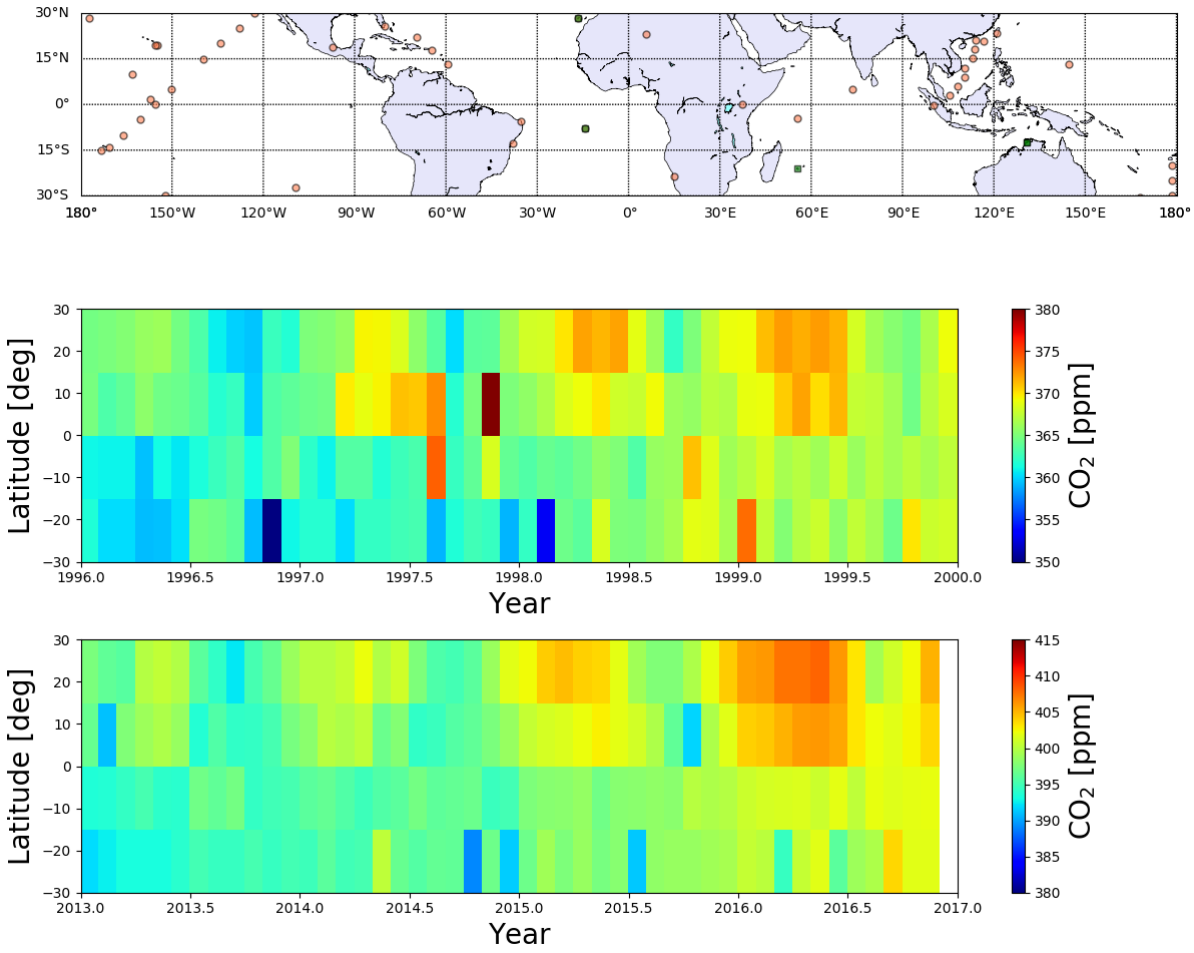

Figure 1 Upper panel: tropical and subtropical distribution of continuous and flask samples of CO_2 from the NOAA Global Greenhouse Reference Network (denoted by circles) and ground-based remote sensing CO_2 column measurements from the Total Carbon Column Observing Network (denoted by squares). Middle and lower panels: Hovmöller diagrams of monthly mean NOAA CO_2 mole fraction measurements described in 15° latitude bins for the 1997/1998 and 2015/2016 El Niño events.

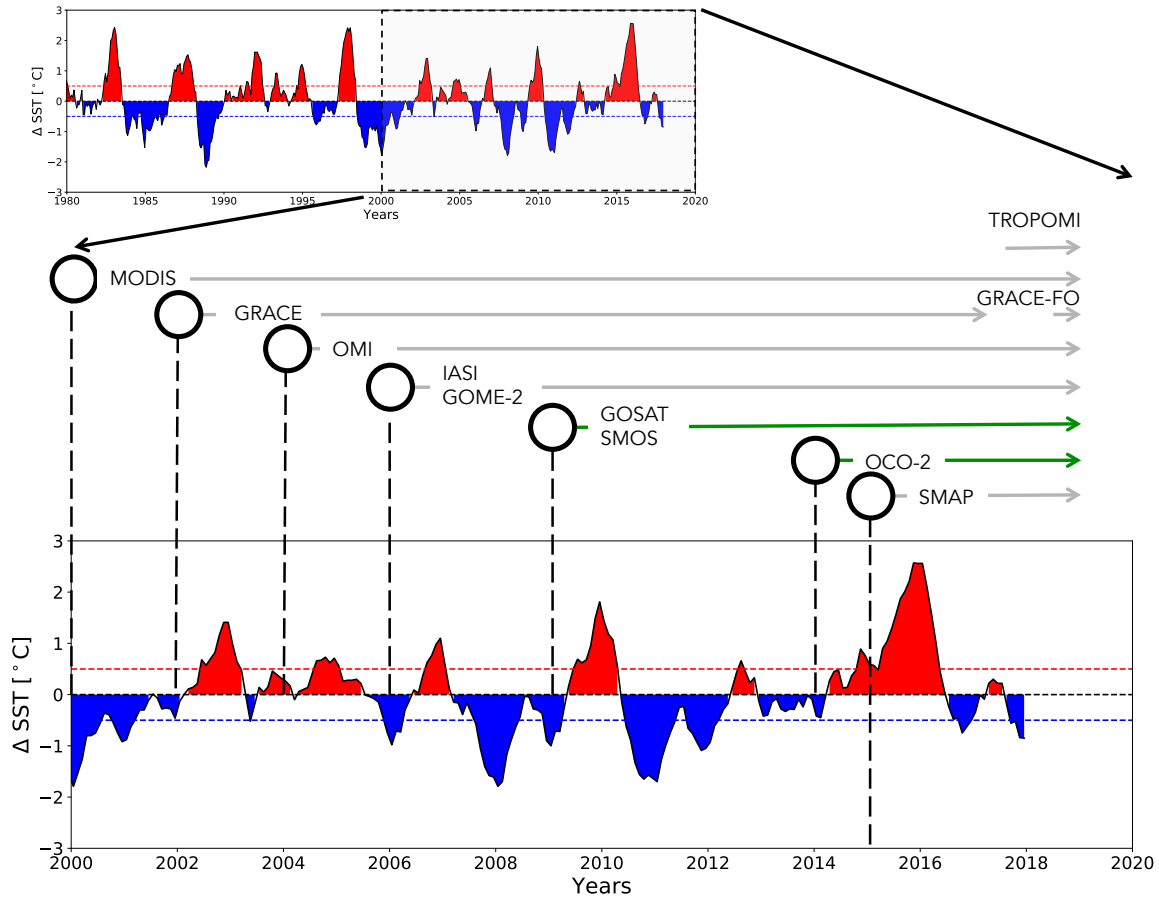

Figure 2 Monthly area averaged SST anomalies over the Niño 3.4 region (5°S-5°N, 170°-120°W) taken from the HadISST1 dataset [Rayner et al, 2003]. Anomalies are calculated by removing the 1951-2000 monthly mean from individual months. A non-comprehensive list of launch dates for satellite instruments relevant to carbon cycle science is also shown. The reader is referred to the main text and Table 1 for further details on individual instruments.

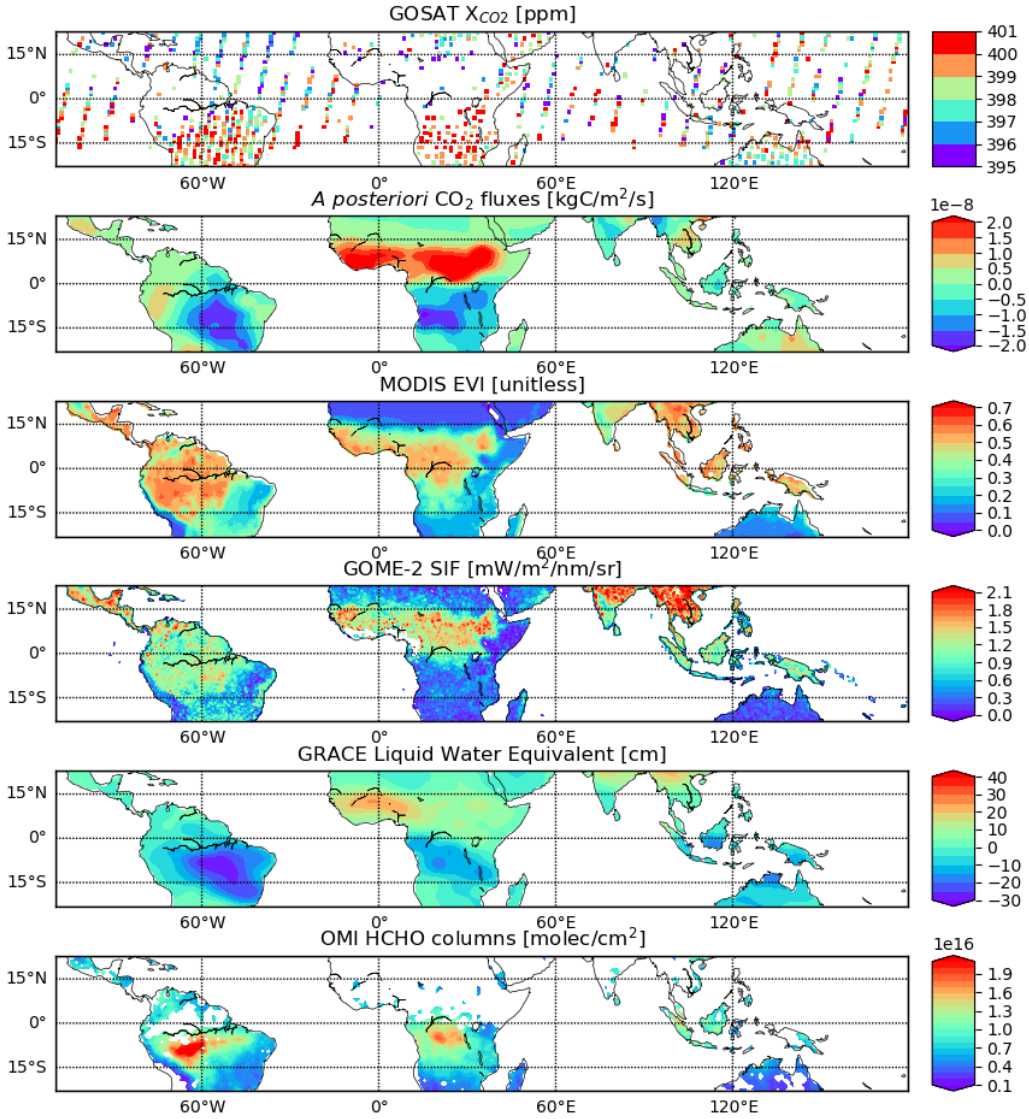

Figure 3 Monthly distribution of GOSAT X_{CO2} data, the corresponding a posteriori CO_2 fluxes, and correlative data for August 2015. Further details of individual datasets are discussed in the main text and Table 1. Data are described on a regular one-degree grid, with the exception of GOME-2 SIF that is described on a regular 0.5-degree grid.

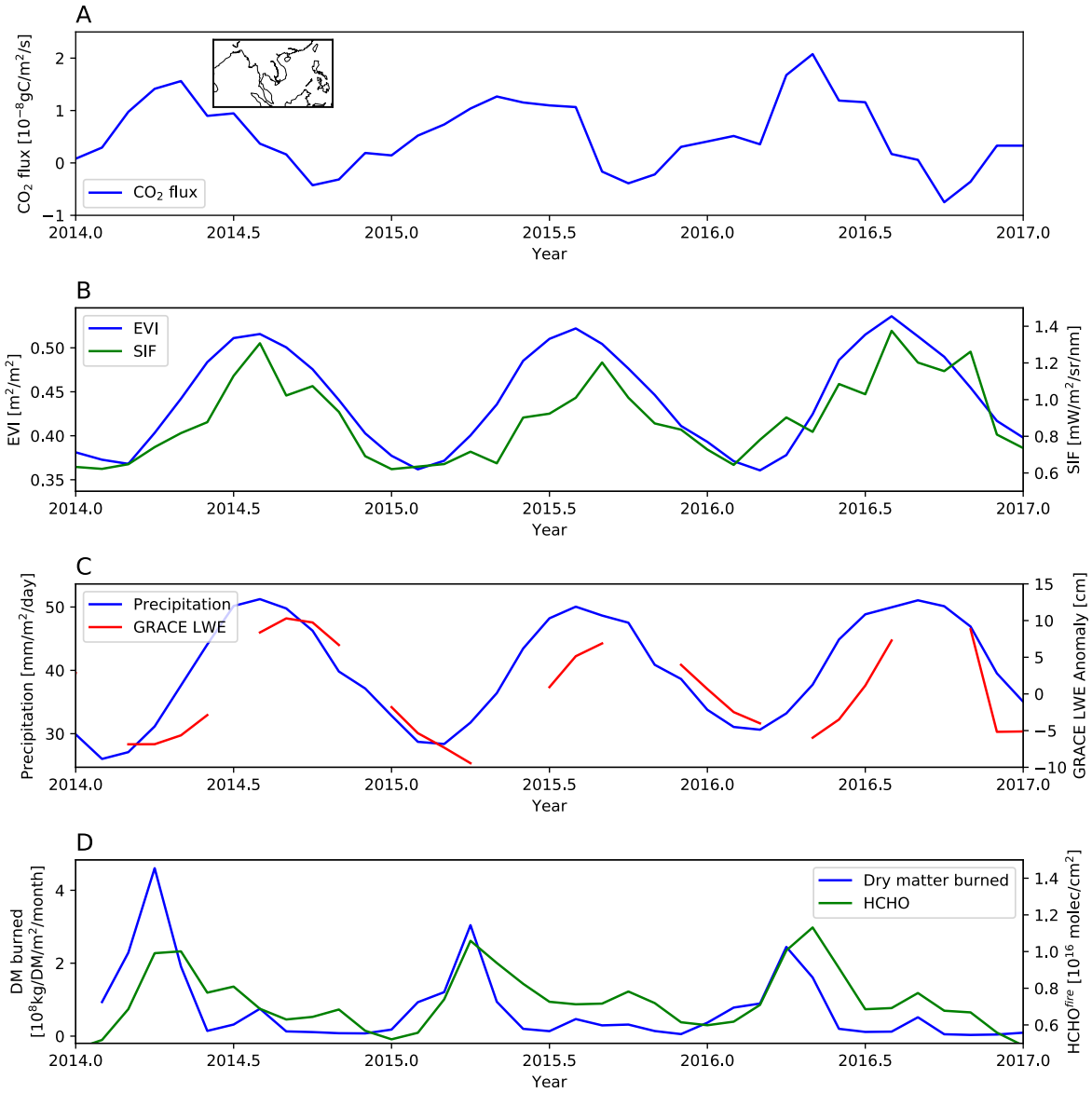

Figure 4 Monthly mean satellite observations over northern tropical Asia, 2014—2017, of A) *a posteriori* CO_2 fluxes inferred from GOSAT X_{CO2} data, B) EVI from NASA MODIS and SIF from GOME-2, C) analysed prepitation fields and LWE thickness anomaly from NASA GRACE, and D) dry matter burned from GFED and HCHO columns from NIVR/FMI OMI with fire-free scenes discarded. The geographical region studied is shown inset of panel A. Further details of individual datasets are discussed in the main text and in Table 1.

Table 1. Summary of key current and future satellite data products that are relevant to the tropical carbon cycle. As much as possible we use values taken from the World Meteorological Organization Observing Systems Capability Analysis and Review Tool: https://www.wmo-sat.info/oscar/. SS and G denote sun-synchronous and geostationary orbits, respectively. We only report one overpass time for instruments that require sunlight for their measurements. *The GRACE data are described using a 300 km Gaussian filter, and we anticipate a similar approach being used by GRACE-FO.

Variable **Satellite instruments**	**Dates**	**Relevant data products**	**Orbit/Local equatorial overpass time**	**Nadir dimension of data product**
Leaf phenology				
MODIS (Moderate Resolution Imaging Spectroradiometer on Terra/Aqua) (+ many instruments)	1999- / 2002-	Leaf area index, fraction of absorbed photosynthetically active radiation	SS/1030 & 1330	500 m
GOME-2 (Global Ozone Monitoring Experiment)	2006-	Solar-induced fluorescence (SIF)	SS/0930	80 km x 40 km
GOSAT (Greenhouse gases Observing Satellite)	2009-		SS/1330	10.5 km diameter
OCO-2 (Orbiting Carbon Observatory)	2014-		SS/1330	1.29 km × 2.25 km
Forest structure				
GLAS (Geoscience Laser Altimeter System)	2003-2010	Forest biomass	Drifting orbit	66 m
ICESAT-1	2003-2008	Vegetation biomass/height	Drifting orbit	40 m
PALSAR/PALSAR-2 (Phased-Array L-band Synthetic Aperture Radar)	2006- 2011/2014-	Forest biomass	SS/1200 & 0000; 91 day repeat	10 m
LandSat-8 onwards	2013-	Forest biomass	SS/1000 & 2200	30 m
Hydrology				
SMOS (Soil Moisture and Ocean Salinity)	2009-	Soil moisture (SM), liquid water equivalent anomaly (LWE)	SS/0600 & 1800	15 km (SM)
SMAP (Soil Moisture Active-Passive)	2015-		SS/0600 & 1800	10 km (SM)
GRACE (Gravity Recovery and Climate Experiment)	2002-2017		SS drifting	1 degree* (LWE)
GRACE-FO (GRACE-Follow on)	2018-		SS drifting	1 degree* (LWE
Atmospheric CO_2				
GOSAT	2009-	Column CO_2, CH_4	SS 1300 common to all	10.5 km diameter
OCO-2	2014-	Column CO_2		1.29 km × 2.25 km
TANSAT (Exploratory Satellite for Atmospheric CO_2)	2016-	Column CO_2		2 km x 2 km
Atmospheric chemistry				
MOPITT (Measurement Of Pollution In The	1999-	CO	SS/1045 & 2245	22 km x 22 km

Troposphere)				
OMI (Ozone Monitoring Instrument)	2004-	HCHO, NO_2	SS/1330	24 km x 13 km
GOME-2	2006-	HCHO, NO_2	SS/0930	80 km x 40 km
IASI (Infrared Atmospheric Sounding Interferometer)	2006-	CO, CH_4	SS/0930	circle diameter 12 km
Sentinel-5P	2017-	HCHO, NO_2, CO, CH_4	SS/1330	7 km x 3.5 km
Fires				
VIRS (Visible and Infra Red Scanner)	1997-2015	Active fire detection (AF), burned area (BA), fire radiative power (FRP)	P	2 km (AF)
VIIRS (Visible/Infrared Imager Radiometer Suite)	2011-		SS/1330	375 m /750 m
MODIS (Terra/Aqua)	1999- / 2002-		SS/1030,2230 & 0130, 1330	0.5 (BA), 1m (AF,FRP)
Himawari-8	2014-		G over Asia	2 km (AF,FRP)
SEVIRI (Spinning Enhanced Visible Infra-Red Imager)	2004-		G over Africa and Europe	3 km (AF,FRP)
GOES (Geostationary Operational Environmental Satellite)	2007-		G over Americas	2.4 km x 4 km (AF,FRP)
Future missions				
Atmospheric CO_2:				
GOSAT-2	~2018	Column CO_2, CH_4	SS	10.5 km
OCO-3	~2019	Column CO_2	Drifting on ISS	1.29 km × 2.25 km
MicroCarb	~2021	Column CO_2	SS	~5 km
Sentinel 5	~2021	Column CO, CH_4	SS	7.5 km x 7.5 km
GeoCarb (Geostationary Carbon Cycle Observatory)	~2022	Column CO_2, CH_4, CO	G over Americas	3 km x 6 km
Forest biomass				
GEDI LiDAR (Global Ecosystem Dynamics Investigation LiDAR)	~2018	Forest biomass/height	Drifting on ISS	25 m
ICESAT-2 (Ice, Cloud and land Elevation Satellite) LiDAR	~2018	Vegetation biomass and height	Drifting orbit	40 m
PALSAR-3	~2020	Forest biomass	SS/1330	5m – 30 m
SAR-L for NASA-ISRO SAR	~2021	Forest biomass/height	SS/0600 & 1800; 12-day repeat	10 – 20 m
BIOMASS	~2022	Forest biomass/height	SS/0600 & 1800; 6-month repeat	50 – 60 m
Fluorescence				
FLEX (FLuorescence EXplorer)	~2022	SIF	SS/1000	300 m